Orbital wave in the Raman scattering cross section of $LaMnO_3$

Purevdorj Munkhbaatar[1,2] and Kim Myung-Whun[1,3,*]

[1]*Institute of Photonics and Information Technology, Chonbuk National University, Jeonju 54896, Republic of Korea*

[2]*Department of Physics, National University of Mongolia, Ulaanbaatar 210646, Mongolia*

[3]*Department of Physics, Chonbuk National University, Jeonju 54896, Republic of Korea*

(Received 30 June 2017; revised manuscript received 19 November 2017; published 1 February 2018)

We calculated the polarization-dependent Raman scattering cross-section spectra of $LaMnO_3$ below the A-type magnetic ordering temperature. Two strong peaks appear around the MnO_6 octahedra stretching phonon frequency. One mode shows A_g symmetry, while the other mode shows B_g symmetry. We found that the A_g symmetry peak is a Jahn-Teller phonon coupled to the orbital wave and the B_g symmetry peak is an orbital wave mode coupled to a Q_2 phonon mode via the Jahn-Teller electron-phonon coupling.

DOI: 10.1103/PhysRevB.97.085101

Raman scattering has provided important information on the quasiparticle excitations in many materials [1]. In strongly correlated electron systems like Mott insulators, identifying the signatures of the nonphonon quasiparticles in the Raman scattering spectra has been attracting long-lasting attentions [1,2]. In a Mott insulator with a single band, the magnetic waves are the renowned nonphonon quasiparticle excitations in the Raman spectra [2]. However, in Mott insulators with multiple active orbitals and the orbital-ordering like $LaMnO_3$, there can be quasiparticles involving the change of orbital state and not involving the spin excitations. Theoretical studies predicted that the orbital wave can appear in such an environment [3–5] and that it may be detected by the Raman scattering measurement [5].

Study of the Raman scattering spectrum of $LaMnO_3$ has revived since the observation of the weak excitations around 150 meV [6]. The peaks were claimed to be due to the orbital wave modes. However, other researchers suspected that the weak signal is due to the first overtones of fundamental phonon modes [7]. Until recently, the 150-meV signals remained controversial despite the accumulation of precise spectroscopic studies for high-quality crystals of $LaMnO_3$ and its relatives [8–11]. The frequency of the orbital wave is linked with the parameters such as the exchange energy and the Jahn-Teller coupling constant, which cannot be directly determined from experiments. The analysis based only on the spectral peak positions in a short frequency range can result in the ambiguous assignments. Careful theoretical analysis based on various experimental facts including the polarization dependence of scattering cross section is necessary for the identification of the scattering peaks and the accurate assignments. Thus far, such work has been rarely performed.

In this paper, we present the simulation results of Raman scattering cross-section spectra for an ideal $LaMnO_3$ in the A-type ferromagnetic ground state. We calculated the polarization dependence of the fundamental modes and the first overtone modes and we compared the calculated Raman spectra with previous experiments. From the comparison, we tried to identify the origins of the peaks. In particular, we focus on the origin of the peak around 611 cm^{-1}.

We adopted Brink's Hamiltonian to calculate the energy dispersion curve and the Raman scattering spectra [12]:

$$H = H_{\rm orb} + H_{\rm e-ph} + H_{\rm ph}. \tag{1}$$

We assumed that the spin degree of freedom is frozen. The first term describes the superexchange interaction between the orbitals:

$$H_{\rm orb} = J \sum_{\langle ij\rangle_\Gamma} T_i^\Gamma T_j^\Gamma, \tag{2}$$

where the sum is over neighboring sites $\langle ij\rangle$ along the $\Gamma = a,b$ crystal axis and J is exchange coupling. The orbital operators T_i^Γ can be expressed in terms of the pseudo-spin-operator (τ): $T_i^{a/b} = (\tau_i^z \pm \sqrt{3}\tau_i^x)/2$, and the plus (minus) sign corresponds to the a (b) axis. The second term of Eq. (1) represents the Jahn-Teller electron-phonon coupling:

$$H_{\rm e-ph} = g \sum_i \left(\tau_i^z Q_{3i} + \tau_i^x Q_{2i}\right), \tag{3}$$

where g is the electron-phonon coupling constant and $Q_{2/3,i}(= a_{2/3,i}^\dagger + a_{2/3,i})$ are phonon operators of Jahn-Teller modes with e_g symmetry. The third term of Eq. (1) is the phonon contribution:

$$H_{\rm ph} = \omega_0 \sum_i (a_{2i}^\dagger a_{2i} + a_{3i}^\dagger a_{3i}) + \omega_1 \sum_{\langle ij\rangle_\Gamma} Q_i^\Gamma Q_j^\Gamma, \tag{4}$$

where ω_0 is the local Jahn-Teller phonon frequency for the Q_2 and Q_3 modes. Here, ω_1 is the nearest-neighbor coupling between the phonons. The $Q_i^{a/b}[= (Q_{3i} \pm \sqrt{3}Q_{2i})/2]$ represents the coupled Jahn-Teller mode along a crystal axis, a or b.

We assumed antiferromagnetic-ordered four Mn-ion e_g orbitals forming two sublattices (A and B) for the unit cell as shown in the inset of Fig. 1(a). To describe the orbital part, we introduce an operator, $\tilde{\boldsymbol{\tau}}_{i\lambda} = (\tilde{\tau}_{i\lambda}^z, \tilde{\tau}_{i\lambda}^x) = (\tau_i^z \cos\theta_\lambda - \tau_i^x \sin\theta_\lambda, \tau_i^x \cos\theta_\lambda + \tau_i^z \sin\theta_\lambda)$, for the λ sublattice. We rewrite the localized pseudo-spin-operators in terms of Holstein Boson

*Corresponding author: mwkim@chonbuk.ac.kr

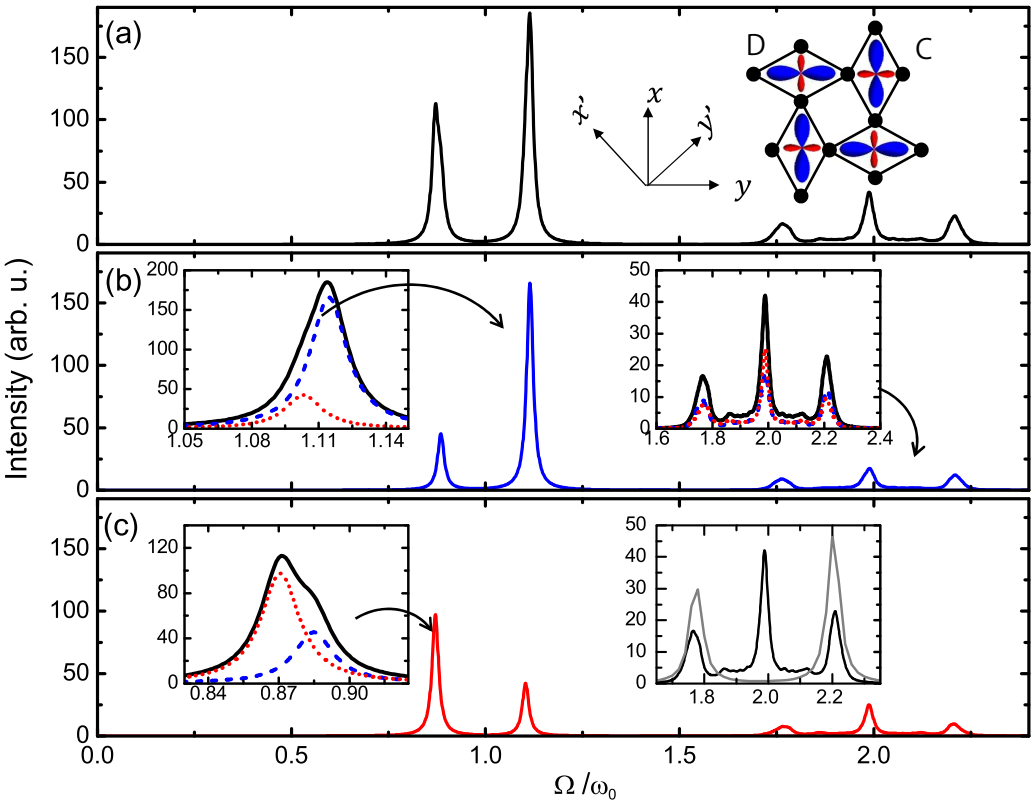

FIG. 1. Raman scattering cross-section spectra for different light polarizations. (a) The spectrum for the (xx) polarization. Inset shows the unit cell lattice, orbital configurations, and the polarization direction with respect to the lattice. (b) The spectrum for the $(x'x')$ polarization. Left inset shows the polarization dependence of the peak at $1.1\omega_0$ [solid line: (xx), dashed line $(x'x')$, and dotted line $(x'y')$]. Right inset shows the polarization dependence of the three peaks near $\Omega/\omega_0 = 2.0$. (c) The spectrum for the $(x'y')$ polarization. Left inset shows the polarization dependence of the peak at $0.9\omega_0$ [solid line: (xx), dashed line $(x'x')$, and dotted line $(x'y')$]. Right inset compares the energy of the peaks near $\Omega/\omega_0 = 1.0$ with that of the three peaks near $\Omega/\omega_0 = 2.0$.

operators (a):

$$\tilde{\tau}_i^{\mathrm{x}} = (a_{1i} + a_{1i}{}^{\dagger})/2, \quad \tilde{\tau}_i^{\mathrm{z}} = (1/2 - a_{1i}{}^{\dagger}a_{1i}). \tag{5}$$

We assumed that the angle on each sublattice is $\theta_{A/B} = \pm\theta$. After inserting the expansion into the full Hamiltonian, Eq. (1) becomes

$$\begin{aligned} H = {} & \omega \sum_i a_{1i}{}^{\dagger}a_{1i} + J/4 \sum_{\langle ij \rangle} \tilde{\tau}_i^{\mathrm{x}} \tilde{\tau}_j^{\mathrm{x}} \\ & + g \sum_i \tilde{\tau}_i^{\mathrm{x}} [\cos(\theta) Q_{2i} \pm \sin(\theta) Q_{3i}] \\ & + \omega_0 \sum_i (a_{2i}{}^{\dagger}a_{2i} + a_{3i}{}^{\dagger}a_{3i}) + \omega_1 \sum_{\langle ij \rangle_\Gamma} Q_i^\Gamma Q_j^\Gamma. \end{aligned} \tag{6}$$

The first term in Eq. (6) is the phenomenological term representing the localized orbiton. Here, ω includes the superexchange interaction and the static Jahn-Teller deformation energy. We assumed that ω is equal to ω_0 (the bare phonon frequency of Jahn-Teller phonon Q_2 mode) under the influence of the strong Jahn-Teller-type electron-phonon coupling. Therefore, the local orbital motion should be locked to the local lattice motion. The plus (minus) sign is for A (B) sublattice. In Eq. (6) we collected only the quadratic terms of boson operators for simplicity [13]. The quadratic Hamiltonian is diagonalized by the Bogoliubov transformation: $\tilde{H} = \sum_{\mu\, \boldsymbol{k}} E_\mu(\boldsymbol{k})\, \alpha_\mu{}^{\dagger}(\boldsymbol{k}) \alpha_\mu(\boldsymbol{k})$. The energy eigenvalues of the transformed Hamiltonian are shown in Fig. 2.

Next, we determined the Raman scattering cross section based on the calculation of the superexchange interaction between neighboring orbital operators by using the Shastry-Shraiman method [14]:

$$\begin{aligned} R(\Omega) = {} & \sum_f \delta(\Omega - (E_f - E_g)) \\ & \times \left| \sum_{\langle ij \rangle_\Gamma} e_{\mathrm{f}\Gamma} e_{i\Gamma} \langle f | \big(1/2 - T_i^\Gamma\big)\big(1/2 - T_j^\Gamma\big) | g \rangle \right|^2. \end{aligned} \tag{7}$$

Here, Ω $(= \omega_i - \omega_f)$ is the Raman scattering energy shift. $E_{g(f)}$ represents the energy of the ground (final) state and $e_{f(i)\Gamma}$ is the scattering (incident) photon polarization vector along the Γ axis.

We obtained the fundamental mode-scattering cross section by collecting the first-order terms of Holstein bosons:

$$\begin{aligned} R_1(\Omega) = {} & \sum_f \delta(\Omega - (E_f - E_g)) \\ & \times \left| \sum_\Gamma e_{\mathrm{f}\Gamma} e_{i\Gamma} \langle f | \sum_i \rho_\Gamma{}^i (a_{1i} + a_{1i}{}^{\dagger}) | g \rangle \right|^2, \end{aligned} \tag{8}$$

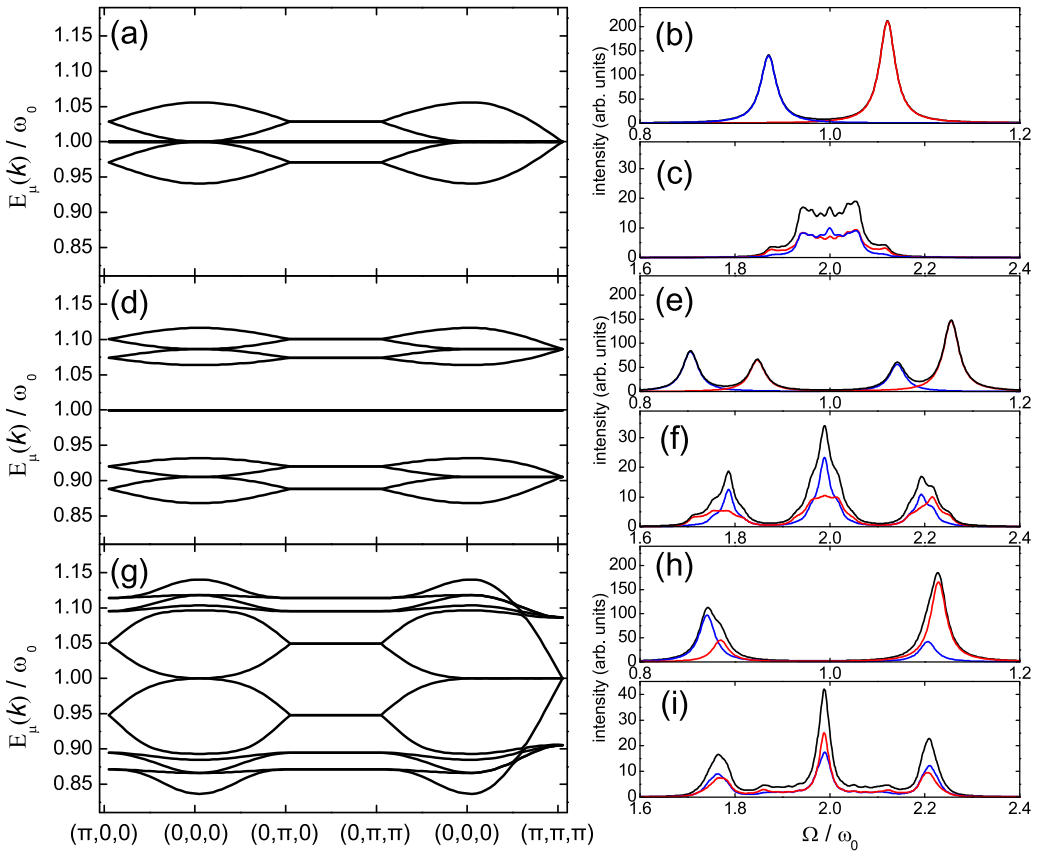

FIG. 2. Dispersion curves [(a), (d), and (g)], the Raman scattering spectra near $\Omega/\omega_0 = 1.0$, i.e., the fundamental mode spectra [(b), (e), and (h)], and the Raman scattering spectra near $\Omega/\omega_0 = 2.0$, i.e, the first overtone mode spectra [(c), (f), and (i)] for different energy parameters. The energy parameters are $J/\omega_0 = 0.5$, $g/\omega_0 = 0$, and $\omega_1/\omega_0 = 0$ for (a), (b), and (c), respectively. $J/\omega_0 = 0.5$, $g/\omega_0 = 0.2$, and $\omega_1/\omega_0 = 0$ for (d), (e), and (f), respectively. $J/\omega_0 = 0.5$, $g/\omega_0 = 0.2$, and $\omega_1/\omega_0 = -0.1$ for (g), (h), and (i), respectively.

with ${\rho_{a/b}}^i = \mp\cos[\pi/6 \mp \theta_\lambda](1 - \sin[\pi/6 \pm \theta_\lambda])$ if $i \in \lambda$ ($\lambda = A$ or B) sublattice. After the Bogoliubov transformation, Eq. (8) becomes

$$\sum_\mu \delta(\Omega - E_\mu(0)) \left| \sum_\nu e_{f\Gamma} e_{i\Gamma} {\rho_\Gamma}^\nu [V_{\nu\mu}(0) + {W_{\nu\mu}}^*(0)] \right|^2. \quad (9)$$

Here, $V_{\nu\mu}(\boldsymbol{k})$ and $W_{\nu\mu}(\boldsymbol{k})$ are Bogoliubov transformation coefficients connecting the boson operator for the νth orbiton in a unit cell to that of the μth eigenmode with the energy $E_\mu(\boldsymbol{k})$ as

$${a_{1\nu}}^\dagger(k) = V_{\nu\mu}(k){\alpha_\mu}^\dagger(k) + W_{\nu\mu}(k)\alpha_\mu(-k). \quad (10)$$

We obtain the scattering cross section of the overtone mode by collecting the second-order terms of Holstein bosons:

$$R_2(\Omega) = \sum_f \delta[\Omega - (E_f - E_g)] \left| \sum_\Gamma e_{f\Gamma} e_{i\Gamma} \langle f | 4 \sum_i {\sigma_\Gamma}^i {a_{1i}}^\dagger a_{1i} + \rho \sum_{i j_\Gamma} (a_{1i} + {a_{1i}}^\dagger)(a_{1j} + {a_{1j}}^\dagger) | g \rangle \right|^2, \quad (11)$$

with $\rho = \cos[\frac{\pi}{6} - \theta]\cos[\frac{\pi}{6} + \theta]$, and ${\sigma_{a/b}}^i = \sin[\pi/6 \mp \theta_\lambda](1 - \sin[\pi/6 \pm \theta_\lambda])$ if $i \in \lambda$ ($\lambda = A$ or B) sublattice. By the Bogoliubov transformation, Eq. (11) becomes

$$\sim \sum_{\boldsymbol{k}\mu\mu'} \delta[\Omega - E_\mu(\boldsymbol{k}) - E_{\mu'}(-\boldsymbol{k})] \left| \sum_{\langle \nu\nu' \rangle_\Gamma} e_{f\Gamma} e_{i\Gamma} \rho [V_{\nu\mu}(\boldsymbol{k}) + {W_{\nu\mu}}^*(\boldsymbol{k})][V_{\nu'\mu'}(-\boldsymbol{k}) + {W_{\nu'\mu'}}^*(-\boldsymbol{k})][1 + \cos(k_\Gamma)] \right.$$
$$\left. + 4 \sum_\nu e_{f\Gamma} e_{i\Gamma} {\sigma_\Gamma}^\nu V_{\nu\mu}(\boldsymbol{k}) {W_{\nu\mu'}}^*(-\boldsymbol{k}) \right|^2. \quad (12)$$

We chose 20×20 lattice cells for the numerical calculations. Figure 1 shows the calculation results for Raman scattering cross sections at the Γ point for the fundamental mode. Figures 1(a)–1(c) show the cases where the polarization

of incident light and scattered light is $(x'x')$, $(x'y')$, and (xx), respectively. As shown in the inset in Fig. 1(a), x and y are the two orthogonal bonding directions of Mn–O–Mn, and x' and y' are diagonal directions, i.e., $x + y = x'(x - y = y')$. In the (xy) polarization, no modes are active.

Before looking at the calculation results, we reviewed some of the points observed in previous experiments: (1) when the polarization of the incident light is the same as the polarization of the scattered light and the direction of the electric field is parallel to the crystal axis [for example, (xx) polarization], Raman experiments using incident light with a wavelength of 632 nm show two strong peaks at 496 and 611 cm^{-1}. The peak at 611 cm^{-1} is more intense than the peak at 496 cm^{-1} [8]. (2) The peak at 496 cm^{-1} has A_g polarization symmetry and the peak at 611 cm^{-1} has B_g polarization symmetry [8]. (3) The peak center frequency is slightly different ($\sim$5 cm^{-1}) depending on the polarizations. For example, at 5 K, the peak center frequency near 496 cm^{-1} is 500 cm^{-1} for the $(x'x')$ polarization and 495 cm^{-1} for $(x'y')$ polarization [11]. (4) There are three peaks near 1200 cm^{-1} whose frequencies are approximately twice as large as 496 and 611 cm^{-1} [6,8,11]. (5) The intensity of the three peaks near 1200 cm^{-1} is approximately 20% of the intensity of the two peaks near 550 cm^{-1} [8]. Our calculation results in Fig. 1 reproduce all of these experimental results.

The energy parameters used to obtain Fig. 1 are $\omega = \omega_0$, $\omega_1 = -0.1\omega_0$, $J = 0.5\omega_0$, $g = 0.2\omega_0$, and $\theta = \pi/2$. If assuming that ω_0 is 557 cm^{-1}, the calculated spectra are consistent with all the five experimental observations listed in the previous paragraph. In Fig. 1(a), there are two strong peaks in the vicinity of $\Omega/\omega_0 = 1$ for (xx) polarization, one at $0.9\omega_0$ and the other at $1.1\omega_0$ (Ω is the measurement frequency). The peak intensity at $1.1\omega_0$ is more intense than that at $0.9\omega_0$. Figures 1(b) and 1(c) show the $(x'x')$ polarization and $(x'y')$ polarization, respectively. The $(x'x')$ polarization spectrum shows a $0.9\omega_0$ peak while the $(x'y')$ polarization spectrum shows a $1.1\omega_0$ peak. The $0.9\omega_0$ peak has A_g symmetry and the $1.1\omega_0$ peak has B_g symmetry, which agrees well with the experiment. However, as can be seen from the experimental results, the symmetry of the two peaks is not perfect.

The $(x'x')$ polarization shows a weak peak at $1.1\omega_0$ and the $(x'y')$ polarization shows a weak peak at $0.9\omega_0$. The cause of the incomplete polarization dependence of the experiment could be an incomplete polarizer or an imperfection of the sample such as crystal twinning. However, our results suggest that even in the ideal experimental situation (ideal crystal and ideal polarizers), the $1.1\omega_0$ peak appears in A_g symmetry and the $0.9\omega_0$ peak appears in B_g symmetry if the Jahn-Teller electron-phonon coupling value is larger than 0. The larger the g value, the greater the intensity of the forbidden symmetry peak. The left inset of Fig. 1(b) and the left inset of Fig. 1(c) show the polarization dependence of the $1.1\omega_0$ peak and $0.9\omega_0$ peak, respectively. It can be seen that the center frequency of the peak is slightly different ($\sim 0.01\omega_0$ corresponding to 5.5 cm^{-1}) for each polarized light, and it is consistent with the experimental results [11].

The calculation shows three relatively weak peaks at $\Omega/\omega_0 = 1.8$, 2, and 2.2. These are first-overtone modes. The scattering intensities of the overtone peaks are almost 20% of the fundamental modes. The polarization dependence of the overtone modes is different from that of the fundamental modes. The intensity of $(x'x')$ polarization is slightly weaker than that of (xx). These results are consistent with the experiments conducted with a 632-nm laser [8,11]. This is because our calculation assumes the Mott-Hubbard transition at 2 eV as the intermediate-state excitation. As shown in the right inset of Fig. 1(c), the calculation shows that the frequencies of the high-energy Raman band cannot be reproduced by simple addition or multiplication of the fundamental mode frequencies. This is also consistent with the experiment [6].

We investigated the dispersion of energy eigenmodes $E_\mu(k)$ for several different energy parameters to understand the origin of the Raman mode peaks. The important parameters are J, g, and ω_1. Figure 2 shows how these three parameters play a role in the scattering cross section. Figures 2(a)–2(c) show the results when $J = 0.5\omega_0$, $g = 0$, and $\omega_1 = 0$. The straight line at $E_\mu(k)/\omega_0 = 1$ represents the dispersion of the Jahn-Teller phonon. The curved lines correspond to the orbital wave modes. J is responsible for the energy bandwidth of the orbiton dispersion. We show the fundamental mode scattering (near $\Omega/\omega_0 = 1.0$) and first overtone scattering (near $\Omega/\omega_0 = 2.0$) signals in Figs. 2(b) and 2(c), respectively. Dispersion curve analysis shows that the peak at $\Omega/\omega_0 = 0.9$ in Fig. 2(b) is a pure orbiton with A_g symmetry, the peak at $\Omega/\omega_0 = 1.1$ is a pure orbiton with B_g symmetry. Both peaks are generated by the superexchange-type interaction between neighboring Mn e_g orbitals. These peaks correspond to the orbital wave or orbiton proposed by Saitoh *et al.* [6]. There is a broad single peak around $\Omega/\omega_0 = 2.0$ and the intensities of those peaks are slightly different for different polarizations.

Figures 2(d)–2(f) show the results for $J = 0.5\omega_0$, $g = 0.2\omega_0$, and $\omega_1 = 0$. Here, g indicates the phonon-orbital coupling by the Jahn-Teller mechanism. The dispersion curves shown in Fig. 2(a) are split and the energy difference between the main curves corresponds to g. The low-energy $[E_\mu(\boldsymbol{k})/\omega_0 < 1]$ curves in the dispersion, correspond primarily to the Q_2-mode Jahn-Teller phonon while the straight line at $E_\mu(\boldsymbol{k})/\omega_0 = 1$ represents the dispersion of the Q_3 mode phonon. The curve at high energy $[E_\mu(\boldsymbol{k})/\omega_0 > 1]$ corresponds to the orbital wave mode. In Fig. 2(e), four scattering peaks appear near $\Omega/\omega_0 = 1.0$. Two more intense peaks are main peaks and the weaker peaks are the satellites. Phonon and orbiton characteristics are mixed in the peaks and the intensities are similar at different polarizations. In Fig. 2(f), three peaks appear near $\Omega/\omega_0 = 2.0$ and the intensities at different polarizations are similar. Any change in g affects the energy difference of the two peaks and the intensity ratio between fundamental and overtone peaks. We chose the g value to meet the value of 20%—the experimentally observed ratio between the fundamental modes and the first overtone modes [8].

Figures 2(g)–2(i) show the results for $J = 0.5\omega_0$, $g = 0.2\omega_0$, and $\omega_1 = -0.1\omega_0$, as the same as those of Fig. 1. Here, ω_1 represents the phonon-phonon interaction between the local phonons. The shape of the curve is very complicated due to the nonzero value of ω_1. However, the scattering peaks are not much different from those of Fig. 2(b), which means that the A_g symmetry peak is from a phonon and the B_g symmetry peak is from an orbiton. However, because g is finite, the orbiton character is mixed in the A_g symmetry peak and that of the phonon is mixed in the B_g symmetry peak. The peak observed at 611 cm^{-1} in the experiment is, therefore, the orbiton coupled

to the phonon through the Jahn-Teller mechanism. Among the three peaks near $\Omega/\omega_0 = 2.0$, the highest-energy peaks are due to a two-orbiton excitation. Middle energy peaks are due to a Q_3 phonon+orbiton excitation. The lowest-energy peak is due to a two-Q_2-phonon excitation.

The last puzzle is the intensity change of each peak depending on the wavelength of incident light. According to the experiment of Krüger *et al.*, when (xx) polarized light with a wavelength of 632 nm is incident, peaks at 496 and 611 cm^{-1} are clearly observed [8]. However, the incident light with a wavelength of about 276 nm still results in the sharp peak at 496 cm^{-1}, but the incident light does not excite the peak at 611 cm^{-1} [8]. We cannot explain the light wavelength dependence, if we assign the peak at 611 cm^{-1} as a simple Mn–O bond stretching phonon mode.

The absorption (or the dielectric function) spectrum of $LaMnO_3$ shows a weak and a broad peak near 2 eV (about 620 nm) and a much stronger absorption above approximately 3 eV (approximately 410 nm) [15,16]. The 2-eV absorption is mainly due to the Mn $3d \rightarrow$ Mn $3d$ interatomic transition, whereas the absorption above 3 eV is mainly due to the O $2p \rightarrow$ Mn $3d$ transition [15]. When the incident photon energy is larger than 3 eV, the O $2p \rightarrow$ Mn $3d$ charge-transfer transition is dominant, and the Raman spectra is dominated by the Franck-Condon process [17]. An incident photon (>3 eV) excites an electron in the initial state of O $2p$ orbital [Fig. 3(a)] and the electron transits to the neighboring Mn $3d$ orbital leaving a hole in the O $2p$ orbital. A hole-doublon state is formed [Fig. 3(b)] and the hole doublon becomes localized because the electron cannot move further to the neighboring Mn e_g orbital. Because of the orbital ordering, the most probable path for the excited electron is the return path to the initial O $2p$ orbital and finally a Mn-O phonon is generated [Fig. 3(c)]. Even after the transition process is complete, the long-range collective orbital configuration cannot be changed very much. As a result, the orbiton cannot be excited, while the Mn-O phonon can be excited. This model explains why the 611-cm^{-1} peak is excited by 632-nm light but not by 276-nm light. The 611-cm^{-1} peak is excited only when the d-d transition occurs.

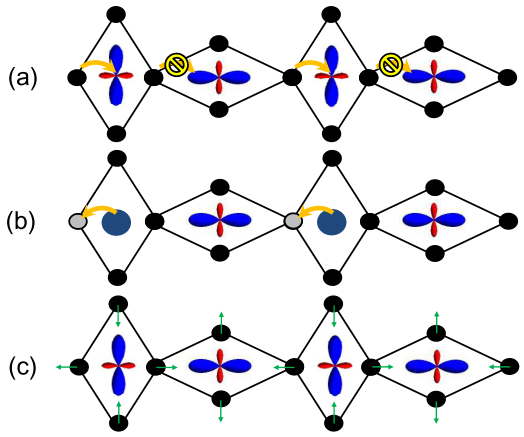

FIG. 3. A schematic diagram for the photon absorption and the Raman mode generation by UV photons of which energy is larger than approximately 3 eV. (a) Initial state: photon absorption causes the electron transition from oxygen ions to Mn ion. Because of the orbital shape, the electron at the specific oxygen can excite at this energy. (b) Intermediate state: the excited electrons move back to the original sites. Scattered photons are generated. (c) Final state: generation of a Raman mode in which energy corresponds to the energy difference between the absorbed photon and the scattered photon. This phonon mode is not coupled to the orbital wave.

In conclusion, our calculations show that the peak at 611 cm^{-1} is an orbiton mode coupled with a phonon. We found that the three peaks near 1200 cm^{-1} (approximately 150 meV), which have been assigned as orbitons in previous studies, do not arise from single orbitons, but are a two-phonon peak (lowest frequency), a phonon-orbiton synthesized peak (middle frequency), and a two-orbiton peak (phonon-coupled, highest frequency).

This research was supported by the National Research Foundation of Korea (Grants No. 2016R1D1A1B03934648 and No. 2016K2A9A1A09914398); by the National Research Foundation of Mongolia (Grant No. SSA 017/2016).

[1] T. P. Devereaux and R. Hackl, Rev. Mod. Phys. **79**, 175 (2007).
[2] G. Blumberg, P. Abbamonte, M. V. Klein, W. C. Lee, D. M. Ginsberg, L. L. Miller, and A. Zibold, Phys. Rev. B **53**, R11930 (1996).
[3] K. I. Kugel and D. I. Khomskii, Zh. Eksp. Teor. Fiz. **64**, 1429 (1973) [Sov. Phys. JETP **37**, 725 (1973)].
[4] M. Cyrot and C. Lyon-Caen, J. Phys. (Paris) **36**, 253 (1975).
[5] S. Ishihara, J. Inoue, and S. Maekawa, Physica C **263**, 130 (1996).
[6] E. Saitoh, S. Okamoto, T. K. Takahashi, K. Tobe, K. Yamamoto, T. Kimura, S. Ishihara, S. Maekawa, and Y. Tokura, Nature (London) **410**, 180 (2001); E. Saitoh, S. Okamoto, K. Tobe, K. Yamamoto, T. Kimura, S. Ishihara, S. Maekawa, and Y. Tokura, *ibid.* **418**, 40 (2002).
[7] M. Grüninger, R. Rückamp, M. Windt, P. Reutler, C. Zobel, T. Lorenz, A. Freimuth, and A. Revcolevschi, Nature (London) **418**, 39 (2002).
[8] R. Krüger, B. Schulz, S. Naler, R. Rauer, D. Budelmann, J. Bäckström, K. H. Kim, S.-W. Cheong, V. Perebeinos, and M. Rübhausen, Phys. Rev. Lett. **92**, 097203 (2004).
[9] L. Martín-Carrón and A. de Andrés, Phys. Rev. Lett. **92**, 175501 (2004).
[10] M. N. Iliev, M. V. Abrashev, H.-G. Lee, V. N. Popov, Y. Y. Sun, C. Thomsen, R. L. Meng, and C. W. Chu, Phys. Rev. B **57**, 2872 (1998).
[11] N. N. Kovaleva, O. E. Kusmartseva, K. I. Kugel, A. A. Maksimov, D. Nuzhnyy, A. M. Balbashov, E. I. Demikhov, A. Dejneka, V. A. Trepakov, and F. V. Kusmartsev, J. Phys.: Condens. Matter **25**, 155602 (2013).

[12] J. van den Brink, Phys. Rev. Lett. **87**, 217202 (2001).
[13] The role of the higher-order terms is just the dynamical screening of the orbital excitation. Also, the first-order terms vanishes because the classical ground state becomes an equilibrium point.
[14] B. S. Shastry and B. I. Shraiman, Phys. Rev. Lett. **65**, 1068 (1990).
[15] M. W. Kim, P. Murugavel, S. Parashar, J. S. Lee, and T. W. Noh, New J. Phys. **6**, 156 (2004).
[16] N. N. Kovaleva, A. V. Boris, C. Bernhard, A. Kulakov, A. Pimenov, A. M. Balbashov, G. Khaliullin, and B. Keimer, Phys. Rev. Lett. **93**, 147204 (2004).
[17] V. Perebeinos and P. B. Allen, Phys. Rev. B **64**, 085118 (2001).